C. AFFOLDERBACH
M. STÄHLER
S. KNAPPE
R. WYNANDS*,✉

An all-optical, high-sensitivity magnetic gradiometer

Institut für Angewandte Physik, Universität Bonn, Wegelerstraße 8, 53115 Bonn, Germany

ABSTRACT Optical magnetometers have reached sensitivities that make them interesting candidates for the measurement of weak magnetic fields also outside physics laboratories. In order to overcome problems with stray magnetic fields a common solution with existing magnetometers is to operate a pair of them in a gradiometer configuration: one sensor measures the signal plus the stray fields, while the other one is mounted such that it is only influenced by the stray fields. In the difference signal the stray fields cancel. We have constructed such a gradiometer consisting of two sensors based on coherent population trapping (CPT) resonances in a thermal cesium vapor. Using a magnetic bias field the intrinsically scalar CPT magnetometer can be turned into a true vector magnetometer that is insensitive to magnetic fields perpendicular to a chosen measurement direction. We describe how to align and calibrate the gradiometer. Stray field suppression by more than two orders of magnitude has been achieved, limited by the sensitivity of the magnetometer. This makes possible the detection of picotesla flux density changes in a weakly shielded or even unshielded environment.

PACS 07.55.Ge; 42.50.Gy; 32.70.Jz; 85.70.Sg; 33.55.Fi

1 Introduction

Static magnetic fields are almost an every-day experience: from the compass (in the days before GPS) to the refrigerator magnet. While in these cases flux densities in the microtesla range are typical, some fundamental physics experiments rely on the measurement and control of magnetic flux densities in the femtotesla range or even less [1]. Important practical applications of low-field magnetometers are the non-destructive testing of materials [2] or the detection of magnetic signals from the human heart [3, 4] or brain [5]. For these purposes superconducting quantum interference detectors (SQUIDs) currently are the only available choice; detection limits for magnetic flux densities lie around $1\,f\,T/\sqrt{Hz}$.

However, SQUID systems have the big disadvantage of requiring cryogenic cooling down to 77 K or even 4 K, with the concomitant problems of material fatigue due to thermal cycling. In contrast, there exist several types of sensitive optical magnetometers that work with an alkali metal vapor at room temperature, thus simplifying operation and reducing power requirements. For instance, early optically pumped magnetometers offered sensitivities around $10\,f\,T$ for $10\,s$ of averaging time [6], with more recent setups reaching $1.8\,f\,T/\sqrt{Hz}$ [7]. Other optical vapor cell magnetometers for the $f\,T$ regime rely on the nonlinear Faraday effect [8]. One prerequisite for the high sensitivities in these experiments is the use of large vapor cells with typical dimensions of 5–15 cm. This makes possible long atom–light interaction times (i.e., small linewidths) and the collection of the signal from a large number of atoms, each driven at low intensity, together with high optical power on the detector.

A common problem for all those magnetometers, when operated outside magnetically shielded enclosures, is presented by stray magnetic fields, which can easily be many orders of magnitude larger than the ones to be measured. While static fields like those from iron beams or nails in walls and furniture can in principle be compensated by compensation coils, a much bigger problem are fluctuating fields. Among these are the short- and medium-term fluctuations of the geostatic field, power line noise at 50 Hz/60 Hz and harmonics, and stray fields from appliances, elevators, and electric street cars. An active compensation of the larger fluctuations is possible [9], at least for the lower Fourier frequencies. However, when the weak field to be measured is produced by a localized source near-by, it is in general more convenient to use a magnetic gradiometer. In the simplest case the gradiometer consists of two identical magnetic field sensors. Sensor 1 is placed as close as possible to the localized magnetic field source and sensor 2 a suitable distance away such that the signal from the source is negligible there. Stray fields from sources sufficiently far away are basically the same at both sensor positions, so in the difference signal the stray fields cancel and only the signal from the weak source remains. Such first-order gradiometers are now standard for SQUID systems, and gradiometers of second or even higher order have been constructed [4].

The gradiometer we are presenting here is based on coherent population trapping (CPT) in a thermal vapor of cesium atoms [10]. It was suggested a few years ago that a CPT-based magnetometer would be immune to power broadening and

✉ Fax: +41-26/300-9631, E-mail: robert.wynands@unifr.ch
New address: Département de Physique, Université de Fribourg, Chemin du Musée 3, 1700 Fribourg, Switzerland

could therefore offer a sensitivity improved by orders of magnitude over existing optically pumped magnetometers [11]. While this prompted us to enter the field it recently turned out that other factors limit the sensitivity of a CPT magnetometer. One of them is the frequency noise of the laser source used to prepare the CPT resonance [12], the other the effect of quantum noise connected to the AC Stark effect [13]. Nevertheless, both for AC [14] and for DC magnetic fields [15] sensitivities around a pT in 1 s of averaging time could be demonstrated for CPT magnetometers, even with characteristic sensor dimensions on the scale of 1 cm and less, so that it makes sense to think about practical applications. This implies the need to study optical gradiometers.

Here we will describe the setup and performance of a magnetic first-order gradiometer based on CPT. A magnetic bias field allows one to constrict the sensitivity to fields along one single spatial direction. Particular emphasis will be placed on how to balance the gradiometer, i.e., how to adjust all parameters such that a homogeneous stray field is optimally suppressed.

2   Coherent dark states

A standard system for the observation of the CPT effect is the three-level Λ system where two ground states are coupled to a common excited state by a bichromatic, near-resonant laser light field. When the difference frequency of the light fields matches the ground state splitting, the atoms are optically pumped into a superposition of the ground states – the coherent dark state. The bichromatic field can no longer excite the atoms out of the dark state, so they are trapped there. The resulting reduction of fluorescence intensity leads to a dark line in the spectrum when the laser difference frequency is scanned [10, 16].

The CPT effect is particularly interesting because the width of the dark resonance line is fundamentally determined by the inverse lifetime of the ground state coherence. This coherence can live for many milliseconds under optimized conditions, leading to narrow resonance lines with steep slopes that can be employed as sensitive frequency discriminators.

3   Scalar and vector gradiometers

A CPT magnetometer measures magnetic flux densities by monitoring the Zeeman splitting of the CPT resonance induced by an external magnetic field. In cesium, the atomic species considered in our experiment, the magnetic sublevels m_4 in the $F = 4$ ground state hyperfine component shift by $\approx 3.5\,\text{Hz/nT} \times m_4$ and those in the $F = 3$ state by $\approx -3.5\,\text{Hz/nT} \times m_3$ (in the linear Zeeman approximation, valid for small flux densities). This means that in a magnetic field Λ systems with many different resonance frequencies can be formed between pairs of ground states. The Zeeman shift of the CPT resonance corresponding to the coupling of $|F = 3, m_3\rangle$ and $|F = 4, m_4\rangle$ is approximately $3.5\,\text{Hz/nT} \times (m_3 + m_4)$ where selection rules forbid all couplings with $|m_4 - m_3| > 2$. Depending on laser polarizations and magnetic field direction up to 21 CPT resonance Zeeman components can be observed in a buffered thermal vapor [17]. Their relative strengths can be calculated in a straightforward way using symmetry considerations [18].

In order to monitor small changes of a magnetic flux density $\boldsymbol{B}_1$ the laser difference frequency is chosen such that it corresponds to the center of the phase profile (index of refraction, see Sect. 4 for experimental details) of the magnetically most sensitive Zeeman component ($\{m_3 = 3, m_4 = 4\}$ for cesium and circular polarization in a field perpendicular to the laser propagation direction, $\{m_3 = 3, m_4 = 3\}$ for a parallel field). The smallest magnetic flux density change that can be detected with a signal-to-noise ratio of unity is

$$\delta B_{\min} = \frac{1\,\text{nT}}{(m_3 + m_4)\,3.5\,\text{Hz}}\frac{\Delta S}{|\text{d}S/\text{d}f|} \tag{1}$$

for the case of cesium vapor. Here f is the laser difference frequency, $\text{d}S/\text{d}f$ the slope of the resonance line at the operating point, and ΔS the noise level there. Obviously, one wants as steep a resonance line as possible, with the lowest possible noise. These issues have been discussed in a previous publication [15]. The sensitivity of the fully optimized CPT magnetometer is shown in Fig. 1, as a function of the detection time constant.

The CPT magnetometer can be operated as a scalar or as a vector magnetometer. Since the shift of the Zeeman levels is directly related to the absolute value of the magnetic field the normal mode of operation is as a scalar magnetometer. A true vector magnetometer, that measures the strength of the magnetic field component along a single direction, is obtained when a sufficiently strong bias field $\boldsymbol{B}_b$ is added along that direction. For simplicity, let us assume that $\boldsymbol{B}_b$ is along the z-direction. The magnetometer response is proportional to the total flux density:

$$|\boldsymbol{B}_{\text{total}}| = |B_b\hat{\boldsymbol{e}}_z + \boldsymbol{B}_1| \tag{2}$$

$$= \sqrt{B_{1x}^2 + B_{1y}^2 + (B_b + B_{1z})^2} \tag{3}$$

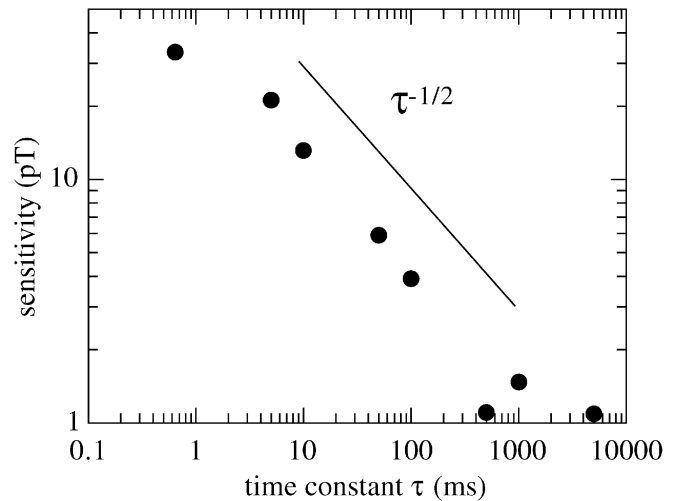$$= B_b\sqrt{1 + 2B_{1z}/B_b + B_1^2/B_b^2}, \tag{4}$$

FIGURE 1   Sensitivity of the CPT magnetometer as a function of the detection time constant τ. Note that the data shown here constitute an improvement by a factor of 3 in sensitivity or a factor of 10 in time resolution over our previously published work [15]

where $\boldsymbol{B}_1$ is the field to be measured. For $B_1 \ll B_b$ the square root can be expanded:

$$B_{\text{total}} \approx B_b + B_{1z} + B_1^2/2B_b. \tag{5}$$

Only the z-component of $\boldsymbol{B}_1$ will therefore influence the output signal of the magnetometer if B_b is sufficiently strong. It is important to note that simultaneously this trick suppresses ambient field noise in the x- and y-directions, leaving only the stray field $B_n \hat{\boldsymbol{e}}_z$ to be taken care of by the gradiometer.

Let us look at the analogous calculation for the gradiometer, in the presence of a homogeneous noise field $\boldsymbol{B}_n$. The two gradiometer sensors are placed at positions $x = 0$ and $x = x_1$ such that a field $\boldsymbol{B}_1(x)$ caused by a localized source near $x = 0$ is negligible at $x = x_1$. The flux density difference ΔB is then given by

$$\Delta B = |\boldsymbol{B}_{\text{total}}(0)| - |\boldsymbol{B}_{\text{total}}(x_1)| \tag{6}$$

$$= \left\{ (B_{1x}(0) + B_{nx})^2 + (B_{1y}(0) + B_{ny})^2 \right.$$
$$\left. + (B_b + B_{1z}(0) + B_{nz})^2 \right\}^{1/2}$$
$$- \left\{ B_{nx}^2 + B_{ny}^2 + (B_b + B_{nz})^2 \right\}^{1/2} \tag{7}$$

$$\approx B_{1z}(0) + \frac{1}{2B_b}(B_1(0)^2 + 2\boldsymbol{B}_n \boldsymbol{B}_1(0)). \tag{8}$$

For a sufficiently large offset field B_b both the influence of homogeneous noise fields and of the transverse components of the localized field are suppressed. It is clear that this suppression will not work as well when the gain for both sensors is different or when $\boldsymbol{B}_n(0) \neq \boldsymbol{B}_n(x_1)$. Also, because of the last term in (8), B_b should be larger than the typical noise fields.

4   Experimental setup

Here we consider the D_2 line of a thermal vapor of cesium atoms, at 852 nm wavelength. The two hyperfine components $F = 3$ and $F = 4$ of the ground state have a frequency splitting of 9.2 GHz, which is then also the nominal laser difference frequency.

The experimental setup can in principle be very compact (Fig. 2). The bichromatic light field is derived from a single diode laser (a vertical-cavity surface-emitting laser, VCSEL). Its drive current is modulated at the full 9.2 GHz hyperfine frequency [19]. The carrier and the upper modulation sideband are tuned to the two hyperfine components of the optical transition, and the carrier is locked to the signal from a DAVLL setup [20] using an auxiliary cesium cell (not shown in Fig. 2). A fast Fourier transform spectrum analyzer can be used to check that the lock point corresponds to the minimum of the detection noise power [21, 22].

The laser beam has a circular cross-section and is split into two parts of equal power. Both beams are circularly polarized. A rotatable half-wave plate in front of the linear polarizer in arm 1 allows for a fine-adjustment of the power in this arm of the gradiometer. Both beams pass through fixed apertures of 2 mm diameter and then through the same Cs cell (length 20 mm) at room temperature, running in parallel, one above the other, with a distance of 15 mm from center to center. No two cesium cells with the same buffer gas pressure were available, so beam diameter and separation had to be chosen so as
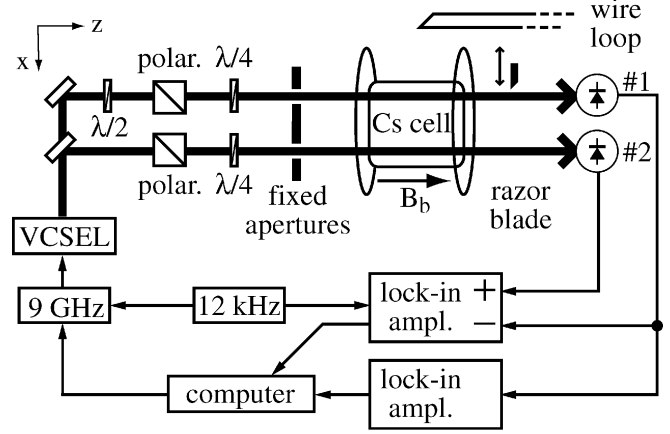

FIGURE 2 Setup of the magnetic gradiometer. The optional half-open magnetic shield around the cell and coil assembly is not shown

to fit the largest-diameter cell available (20 mm here). A drawback of the small beam diameter here is that the single-arm magnetometric sensitivity is significantly reduced compared to Fig. 1. The steepness of the dark-resonance slope and thus the magnetometric sensitivity is increased by using 8.7 kPa of neon as a buffer gas in the cell. The frequent Cs-Ne collisions impede the motion of the Cs atoms out of the laser beam, thus increasing the interaction time and narrowing the linewidth [23]. In addition, the buffer gas effectively localizes the Cs atoms so that they cannot travel from one laser beam to the other within the lifetime of their ground state coherence. Therefore, the effects due to atoms interacting with both beams are negligible.

Behind the cell, beam 1 is attenuated by pushing in a razor blade from the side with the help of a micrometer stage. Both beams are focused onto photodiodes. In order to increase the signal-to-noise ratio the 9 GHz − frequency is itself frequency-modulated at 12 kHz and the photodiode signals are demodulated by lock-in amplifiers. This lock-in detection also provides the desired phase response of the atomic vapor in the quadrature output.

CPT resonance spectra are taken by scanning the 9 GHz modulation frequency around its nominal value. After demodulation of the detected signal the line shape for each of the arms is the sum of three copies of the intrinsic dispersion line shape of the CPT resonance: one for the carrier in the center and one each for the two first-order kHz-modulation sidebands, displaced to each side by the modulation frequency [24]. The steep slope at the center of the kHz-carrier is used as a discriminator for the detection of the Zeeman shift: if, for example, the 9 GHz modulation frequency is held fixed at the line center the output signal of the lock-in amplifier is proportional to the magnetic flux density change. Then the optimum operating point for the laser difference frequency in terms of the sensitivity of each arm is right at the center of the dispersive line shape, where the slope is at its maximum.

In order to isolate and monitor only the most sensitive Zeeman component a homogeneous bias field $B_b \approx 0.5\,\mu\text{T}$ is applied along the z-direction. For gradient fields on the nanotesla scale one is therefore well within the operating regime as a vector magnetometer/gradiometer along the z-direction.

For gradiometer operation the photodiode signals are demodulated by one single lock-in amplifier in differential input mode, whose output then constitutes the gradiometer signal. Because the light fields for both gradiometer arms are derived from the same laser, the laser noise contributions limiting the magnetometer sensitivity [15] cancel to a large extent in this detection scheme. The signal from photodiode 1 is simultaneously fed into a second lock-in amplifier whose output signal can be used to lock the gradiometer to the point of maximum sensitivity, as explained below.

In order to apply calibrated test gradients one could take advantage of one of the many sophisticated gradient coil arrangements with large working distances that have been developed for magnetic resonance imaging. For a test of our gradiometer, however, a much simpler setup is sufficient. A gradient of the z-component of $\boldsymbol{B}_{total}$ can be applied between the two gradiometer arms with the help of a rectangular loop of wire (length 100.5 cm, width 21.5 cm) suspended 15.0 cm above the center of the Cs cell such that one of the short sides is centered over the cell and runs perpendicular to the laser beams. This stretch of wire has the strongest effect on the total field strength at the position of the cell, with the contributions by the long sides being smaller and also mostly cancelling each other. The wire loop has to be closed as far away from the cell as possible; otherwise, the field contributions by the two short sides of the rectangle will partly cancel, as well.

In this way inhomogeneities of the field gradient are kept below the detection level. A loop current of 1 mA leads to a field difference of about 110 pT between the laser beams, accompanied by an additional offset field of 660 pT for both beams. Optionally, the whole setup can be surrounded by a single-layer mu-metal shield which is open on one side.

5   Modes of operation of the gradiometer

In the ideal gradiometer the line shapes and amplitudes in the two arms are identical, so that their difference is precisely zero when no magnetic gradient is present. When now the resonance lines in the two beams are shifted with respect to each other by a magnetic field gradient, a peak appears in the gradiometer line shape whose amplitude is proportional to the field gradient (Fig. 3c). With the laser difference frequency set to its operating point at the line center, the amplitude of this peak can be read directly from the output of the lock-in amplifier operated in differential input mode. The range of linear response is then limited by the linearity of the single-arm line profile around the operating point. A common-mode field change, on the other hand, causes identical line shifts in both arms and therefore will not produce any gradiometer signal, as long as the line shapes are identical over the frequency range covered by the line shifts.

Strictly speaking, it is only required that right at the operating point the signals from the two gradiometer arms are the same: as soon as a difference signal is detected a servo loop could apply a compensating gradient field to keep the gradiometer always locked to its operating point. While this mode of operation in principle provides a linear gradiometer response over an unlimited range of field gradients it has two potentially serious drawbacks: First of all, it requires a servo loop with a bandwidth higher than the signals to be measured,
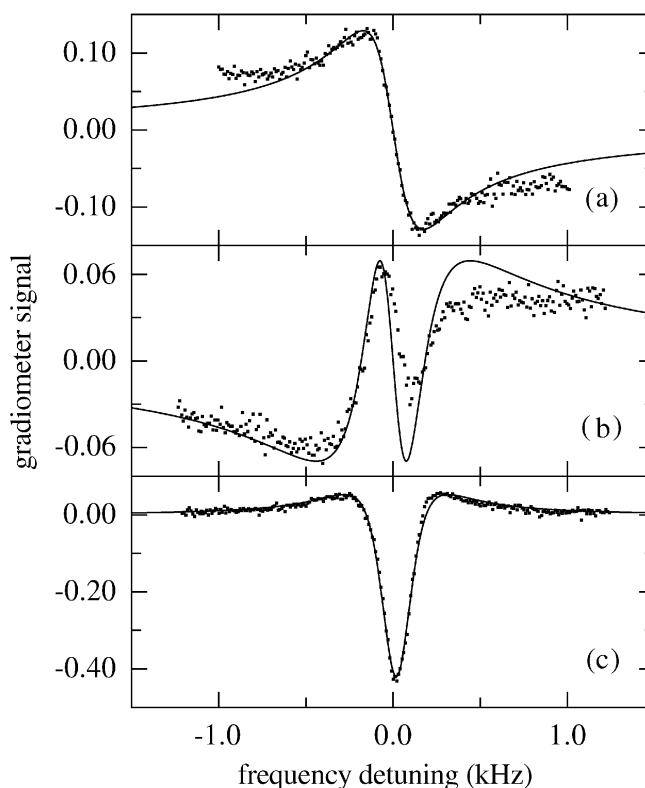

FIGURE 3   Some examples of the line shapes in a well-balanced gradiometer when only one parameter is slightly mismatched. **a** Amplitude in arm 1 too small by 13%; **b** width in arm 1 too large by 15%; **c** position in arm 1 blue-shifted by 11% of the linewidth. The maximum amplitude in arm 2 is normalized to unity in all cases. The *solid lines* are calculations using the experimental parameters. The lock-in amplifier time constant is 100 ms for these and all following figures

which means that also the noise within that larger bandwidth is collected, thus reducing the sensitivity. In addition, a carefully calibrated gradiometer coil is needed to precisely compensate the external gradient. Not only does this increase the complexity of the setup but also might this complete compensation of the gradient produced by the localized source be undesirable, depending on the application. Furthermore, a well-balanced gradiometer offers much better suppression against large common-mode excursions faster than the servo loop. It is therefore preferable to use precisely matched line shapes in the two arms so that the operating point of this balanced gradiometer can be allowed to change in response to an external gradient.

For optimum common-mode noise suppression by the gradiometer the linear slopes in the line shapes have to be the same for both gradiometer arms. Under our operating conditions, the 12-kHz-carrier component of the lock-in line shape is very well represented by a dispersive lorentzian, sitting on a small constant background, and the gradiometer output line shape is the difference of two such lorentzians. Therefore in the experiment the balancing requirement can be met by carefully matching both the amplitude and the linewidth of the two signals; for lorentzian line shapes in both arms this is equivalent to balancing the slopes. As soon as one or both of the resonance lines are Zeeman-shifted too far from the nominal operating frequency, so that the curvature of the line shape causes a noticeable deviation from the linear slope at

the line center, the linearity of both the common-mode and the gradiometer signal will be degraded. Therefore also the line centers of each arm should be at exactly the same position, which means that residual static gradients must be compensated. This also removes static offsets of the gradiometer output signal and maximizes the range of linear response. A calibration of the balanced gradiometer signal is obtained from the maximum line amplitude in a series of data similar to that of Fig. 3c for different field gradients of known amplitude. The uncertainty of this calibration factor sums to about 7% for the data reported here.

Large common-mode field changes can drive the operating point far out into the line wing where the gradiometric sensitivity is essentially zero. In the current setup, this would happen for common-mode flux density changes of about 10 nT, determined by the single-beam linewidth. To make the gradiometer robust against even larger common-mode excursions, the laser difference frequency can be locked to the center of one of the single-beam resonances by using the signal from photodiode 1 and the second lock-in amplifier. The servo loop is closed by computer control of the laser modulation frequency; thus the bandwidth is limited by the speed of the GPIB interface bus. For large and quickly-varying common-mode excursions this servo bandwidth can be increased in principle by replacing the computer-controlled rf generator by a voltage-controlled oscillator or by a synthesizer with a tunable external reference oscillator. Again, also in this operation mode a well-balanced gradiometer provides a better suppression of common-mode excursions on timescales faster than the servo loop.

Optimum gradiometer signal amplitude and output linearity can be guaranteed when the laser difference frequency is locked exactly half-way between the line centers of the two single-beam resonances, making the operating point stay on the center of the gradiometer line shape. This can be achieved by locking to the center of the sum of the signals, increasing both signal and noise for the common-mode servo at the same time. This more complicated way of locking was not implemented for the experiments reported here, since from the experimental parameters the reduction and nonlinearity of the gradiometer signal even for the simple servo loop can be estimated to be only about 1%.

6   Balancing the gradiometer

Due to small imperfections in the experimental setup, the lorentzians in the two arms of the gradiometer can in general have slightly different amplitudes, widths, and positions. It is essential that these small differences are trimmed away when the large common-mode suppression reported here is to be achieved. Otherwise, at this level even tiny differences in beam position, laser power, or even a temperature gradient across the cell can compromise the gradiometer performance. This problem is exacerbated when two separate vapor cells are used to obtain a larger sensor spacing. The balancing procedure then also has to compensate for potentially slightly different temperatures, buffer gas pressures, or cell lengths.

It is not obvious how to adjust the experimental parameters such that the three line shape parameters are simultaneously balanced for both arms. For instance, changing the power in one beam in order to adjust the signal amplitude also changes the width due to power broadening and the position due to the light shift. In a phenomenological approach we have therefore examined the suitability of several experimental parameters with respect to an easy and reproducible balancing of the gradiometer: laser power, beam diameter or shape, power on the detector, detector gain, and an additional magnetic field gradient. In the end, it turned out that the best combination is the triplet of parameters: (1) the power in each arm; (2) the power reaching the photodiodes; (3) the additional magnetic field gradient.

The gain of the photodiode amplifiers was found to be hard to use as an adjustment parameter because for a reasonably simple circuit a gain change was also accompanied by a phase change, which made the differential detection by the lock-in amplifier difficult (with our model the reference phase must be the same for both inputs).

Although these parameters are not orthogonal to each other a reliable balancing can nevertheless be obtained. For a first coarse adjustment, already with the longitudinal bias field B_b applied, the laser difference frequency is tuned such that the magnetically insensitive dark resonance corresponding to the coupling of $|F = 4, m_4 = 0\rangle$ and $|F = 3, m_3 = 0\rangle$ is observed. The overall laser power is optimized such that a maximum magnetometric sensitivity is obtained for arm 2 [15]; the lock-in amplifier is operated in single-input mode for this purpose. After that, the amplitude of the dark resonance line in arm 1 is matched to that of arm 2 by adjusting the position of the razor blade in front of photodiode 1 and observing the two individual line shapes separately, for instance by using one lock-in amplifier for each photodiode signal. Then the widths are equalized by rotating the half-wave plate in arm 1. This requires some readjustment of the razor blade's position, in a process that converges quickly. In the next step, the magnetically sensitive resonance component ($|F = 4, m_4 = 3\rangle$ coupled to $|F = 3, m_3 = 3\rangle$) is selected by changing the laser difference frequency. Now the current through the wire loop is adjusted to make the dark resonances in both arms appear at the exact same position on the difference frequency axis. Finally, the lock-in amplifier is switched to differential mode and all three parameters are fine-tuned one last time, guided by the characteristic shapes of the slightly misbalanced difference signals (Fig. 3). Since the sign of the gradiometer line shapes indicates the sign of the mismatch an optimum is quickly reached.

It is very convenient that the central features in Fig. 3b,c are narrower than that in Fig. 3a, which is also the width of the resonance in a single arm. For instance, during the balancing procedure it can happen that both the amplitudes and the widths in the two arms are different in a way that makes the wings of the resulting gradiometer line shape flat, leaving only a narrow dispersive feature in the center. The width of this feature helps to distinguish this situation from the case where only the amplitudes are different, like in Fig. 3a.

For a quantitative assessment of the gradiometer performance it is helpful to define the common-mode suppression ratio R. This is the voltage signal change $s\delta$ for a given line shift δ in one gradiometer arm divided by the voltage signal change $s_d\delta$ in the difference signal. Here $s = 4a/\gamma$ is the
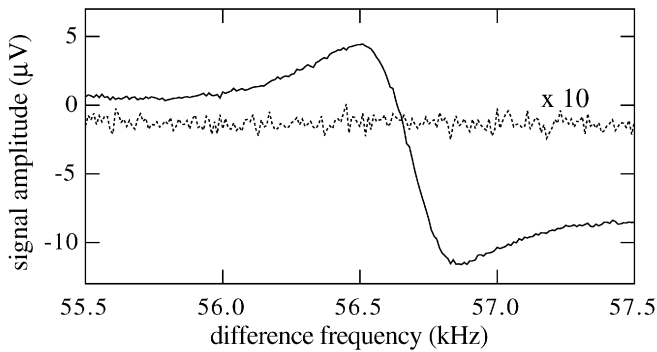
FIGURE 4 Resonance line shape for one gradiometer arm only (*solid curve*) and well-balanced difference signal (*dotted curve*, voltage signal expanded by a factor of ten). From the curves a balancing of the line slopes in the two arms of at least 6×10^{-3} is deduced, corresponding to common-mode suppression by a factor of 167

slope at the line center for a lorentzian line shape from one gradiometer arm of known width γ and amplitude a, and s_d is the slope of the difference signal, equal to the difference of the single-beam line slopes. Thus for equal linewidths the common-mode suppression can be re-expressed as $R = s/s_d = a/a_d$ in terms of the amplitude a_d of the difference signal, which is easy to read from the experimental data (like the one in Fig. 3a).

The dotted curve in Fig. 4 shows the resulting flat difference spectrum for optimized balancing of the two arms in our gradiometer, while the solid curve gives the corresponding signal from one gradiometer arm only. Amplitudes in the two arms are $a_1 = a_2 = 7.9\,\mu\text{V}$, and $U_{\text{rms}} = 47\,\text{nV}$ for the gradiometer trace. From this one obtains a lower limit for the common-mode suppression ratio of $R \geq 167$. This ratio is limited by our ability to detect small changes of the output signal during the balancing procedure, i.e., the magnetometric sensitivity of the setup. While in principle it would be possible to improve the balance even more, using longer integration times, and therefore to obtain lower U_{rms}, this would not be useful for measurements with the shorter time constant, because this improvement would be masked by the detection noise, unless very strong common-mode signals are expected.

One should note that the balancing algorithm developed here also compensates other imperfections in the setup, like unequal photodiode efficiencies or slightly different gains in the two inputs of the lock-in amplifier. Although using the $|F = 4, m_4 = 0\rangle$ to $|F = 3, m_3 = 0\rangle$ transition for the first coarse adjustment is especially helpful in magnetically noisy environments, this is not strictly necessary. In some cases even these resonance lines can be shifted against each other due to, e.g., temperature gradients across the cell. Then it is better to switch to the magnetically sensitive resonance component right after a coarse balancing of the gradiometer. Otherwise, the peak due to the non-identical line positions (Fig. 3c) will dominate the line shapes during the fine-adjustment of the other parameters.

7   Gradiometer performance

The gradiometer was set up inside a large cylindrical magnetic shield (diameter 59 cm, length 90 cm, wall

thickness 1.3 mm) with a cover on one end that leaves a 3.5 cm diameter opening for the pair of laser beams. The shield provides some suppression of large common-mode field fluctuations that would otherwise exceed the acceptable range in the unlocked mode, as explained above, and therefore makes balancing the gradiometer much easier. Furthermore, the shield also guarantees a sufficient homogeneity of the remaining background field over the sensor volume (most of the strong field inhomogeneity is produced by equipment that cannot be moved more than 1–2 m away in our small laboratory). Otherwise the resonance lines are additionally broadened, which reduces the magnetometric sensitivity. In fact, inhomogeneities of the background field are known to be limiting the performance also of other types of gradiometers in unshielded environments [4]. In our experiment the shield proved to be not strictly necessary: a preliminary version of the gradiometer was operated outside the shield and provided a factor of 20 suppression of ambient field fluctuations. The absolute sensitivity of this preliminary setup was indeed limited by the field inhomogeneity.

In Fig. 5 a time series illustrates the common-mode suppression effect. Large excursions of the ambient magnetic field in our laboratory are strongly suppressed. For a more quantitative evaluation, calibrated steps of up to 21 nT were applied to the bias field B_b, well reflected in the output signal of a single arm of the gradiometer (lower trace in Fig. 6).
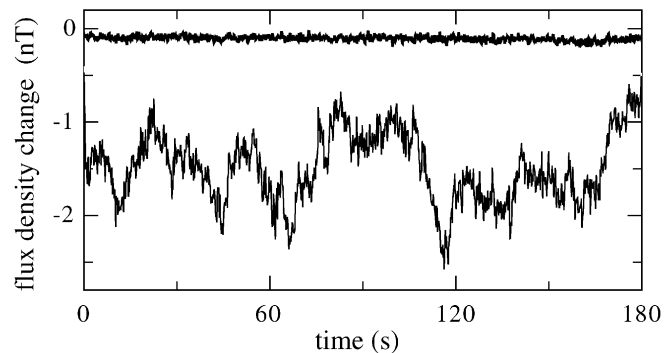

FIGURE 5 Time series of the gradiometer output signal (*upper, flat trace*) and the signal from one of the arms only (*lower, fluctuating trace*). The operating point was not locked to the common-mode field here
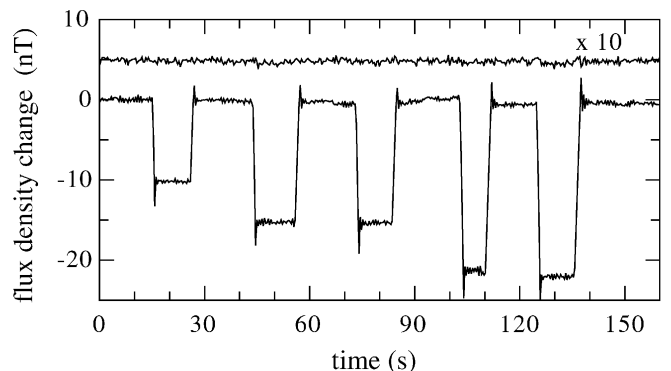

FIGURE 6 Gradiometer output signal (*upper trace*, expanded by a factor of ten) for jumps of the external bias field of 10, 15, and 21 nT (*lower trace*, derived from the laser difference frequency controlled by the common-mode servo loop). No common-mode signal can be observed in the gradiometer signal. This gives a lower limit for the common-mode suppression ratio of at least 800

Because these common-mode steps exceeded the operating range given by the linewidth, the laser difference frequency was locked to the center of the resonance line for this measurement. The corresponding gradiometer signal (upper trace in Fig. 6) does not show any effect larger than the rms (root-mean-square) noise level, corresponding to a gradiometric sensitivity of 26 pT at a time constant of 100 ms. Taking this value as the minimum detectable field change results in a factor of 808 as the lower limit for the suppression ratio of common-mode field changes in this locked operation mode.

The gradiometric sensitivity derived from the noise level was checked directly by applying well-defined test gradient steps of 23 pT/mm, corresponding to a total flux density difference of 347 pT, using the wire loop above the Cs cell. Again, the laser difference frequency was locked to the optimum operating point for the measurement. The resulting steps in the gradiometer output signal (Fig. 7) have a signal-to-noise ratio of about 14, in agreement with the extrapolated sensitivity given above. The smallest detectable flux density change in one arm of the gradiometer relative to the other is only 26 pT. This is about a factor of 1.5–2 better than the 35–55 pT sensitivity obtained when one arm of the gradiometer setup is operated as a stand-alone magnetometer (the actual sensitivity is hard to measure in a basically unshielded laboratory environment). This is due to the cancellation of a major contribution to the detection noise: fluctuations of the laser power on the detector, produced by the demodulation of laser frequency fluctuations on the slope of the Doppler-broadened atomic absorption profile [22]. These are obviously correlated in the two gradiometer arms.

There are several ways to improve the magnetometric sensitivity of the gradiometer in future experiments. First of all, while the small beam diameters in our setup increase the spatial resolution, they also limit the total power on the photodiodes (for a given intensity in the vapor cell) and therefore the signal-to-noise ratio. Furthermore, the small beam size also increases the resonance linewidth due to time-of-flight broadening. Because both beams in our experiment were running close to the cell walls the ground state relaxation rate is increased, broadening the resonance as well. Both effects reduce the sensitivity and could be avoided by using larger vapor cells. Increased laser beam diameters would also increase the sensitivity, as long as sp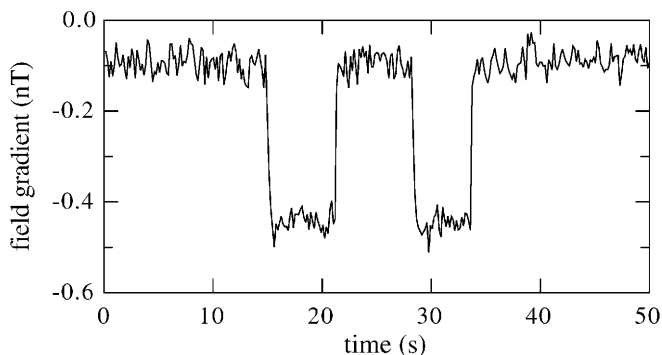atial inhomogeneities of the external field over the interrogation volume do not broaden the resonance line too much. Alternatively, a shorter but slightly heated cell would provide a better sensitivity [25], but without the drawback of increased sensitivity to field inhomogeneities. Furthermore, the contrast of the CPT resonance is limited by the fact that on the D_2 line of Cs there are the $F = 2$ and $F = 5$ hyperfine components of the excited state which cannot form Λ systems with the ground state components and therefore cause one-photon losses. Recent results with rubidium show that under otherwise comparable conditions these losses can be avoided on the D_1 line and the sensitivity is increased by about a factor of ten [26]. Still another approach is to use cells with an anti-relaxation wall coating. Motional narrowing [27] will reduce the broadening due to field inhomogeneities within the interrogation volume in this case.

8 Conclusion

The sensitivity of our CPT-based gradiometer should be large enough for some interesting applications like magnetocardiography when the changes to the experimental setup discussed above are implemented. The sensor can be miniaturized, similar to the case of a dark-resonance clock: we have built a prototype frequency standard where the complete optical setup fits into a box with the size of a finger [28]. Such a sensor would be very robust because the VCSELs do not need any external optics to define their output wavelength, any spatial orientation could be chosen, and convenient operation at room temperature would be possible.

FIGURE 7 Gradiometer output signal for a 23 pT/mm step of an external gradient

REFERENCES

1 L.R. Hunter: Science **252**, 73 (1991)
2 Y. Zhang, Y. Tavrin, H.-J. Krause, H. Bousack, A.I. Braginski, U. Kalberkamp, U. Matzander, M. Burghoff, L. Trahms: Appl. Supercond. **3**, 367 (1995)
3 G.M. Baule, R. McFee: Am. Heart J. **66**, 65 (1963)
4 S.J. Williamson, L. Kaufman: J. Magn. Magn. Mater. **22**, 129 (1981)
5 M. Hämäläinen, R. Hari, R. Ilmoniemi, J. Knuutila, O.V. Lounasmaa: Rev. Mod. Phys. **65**, 413 (1993)
6 C. Cohen-Tannoudji, J. Dupont-Roc, S. Haroche, F. Laloë: Phys. Rev. Lett. **22**, 758 (1969)
7 E.B. Aleksandrov, M.V. Balabas, A.K. Vershovskii, A.E. Ivanov, N.N. Yakobson, V.L. Velichanski, N.V. Senkov: Opt. Spectr. **78**, 292 (1995)
8 D. Budker, D.F. Kimball, S.M. Rochester, V.V. Yashchuk, M. Zoloterev: Phys. Rev. A **62**, 043403 (2000)
9 L.A. Marzetta: Rev. Sci. Instrum. **32**, 1192 (1961)
10 E. Arimondo: Prog. Opt. **35**, 257 (1996)
11 M.O. Scully, M. Fleischhauer: Phys. Rev. Lett. **69**, 1360 (1992)
12 S. Knappe, R. Wynands, J. Kitching, H.G. Robinson, L. Hollberg: J. Opt. Soc. Am. B **18**, 1545 (2001)
13 M. Fleischhauer, A.B. Matsko, M.O. Scully: Phys. Rev. A **62**, 013808 (2000)
14 A. Nagel, L. Graf, S. Naumov, E. Mariotti, V. Biancalana, D. Meschede, R. Wynands: Europhys. Lett. **44**, 31 (1998)
15 M. Stähler, S. Knappe, C. Affolderbach, W. Kemp, R. Wynands: Europhys. Lett. **54**, 323 (2001)
16 G. Alzetta, A. Gozzini, L. Moi, G. Orriols: Il Nuovo Cim. B **36**, 5 (1976)

17 S. Knappe, W. Kemp, C. Affolderbach, A. Nagel, R. Wynands: Phys. Rev. A **61**, 012504 (2000)
18 R. Wynands, A. Nagel, S. Brandt, D. Meschede, A. Weis: Phys. Rev. A **58**, 196 (1998)
19 C. Affolderbach, A. Nagel, S. Knappe, C. Jung, D. Wiedenmann, R. Wynands: Appl. Phys. B **70**, 407 (2000)
20 K.L. Corwin, Z.-T. Lu, C.F. Hand, R.J. Epstain, C.E. Wieman: Appl. Opt. **37**, 3295 (1998)
21 J. Kitching, L. Hollberg, S. Knappe, R. Wynands: Opt. Lett. **26**, 1507 (2001)
22 J. Kitching, H.G. Robinson, L. Hollberg, S. Knappe, R. Wynands: J. Opt. Soc. Am. B **18**, 1676 (2001)
23 S. Brandt, A. Nagel, R. Wynands, D. Meschede: Phys. Rev. A **56**, R1063 (1997)
24 G.C. Bjorklund, M.D. Levenson, W. Lenth, C. Ortiz: Appl. Phys. B **32**, 145 (1983)
25 S. Knappe, J. Kitching, L. Hollberg, R. Wynands: Appl. Phys. B **74**, 217 (2002)
26 M. Stähler, R. Wynands, S. Knappe, J. Kitching, L. Hollberg, A. Taïchenachev, V. Yudin: Opt. Lett. **27**, 1472 (2002)
27 S.F. Watanabe, H.G. Robinson: J. Phys. B Atom. Molec. Phys. **10**, 931 (1977)
28 J. Kitching, L. Hollberg, S. Knappe, R. Wynands: Electron. Lett. **37**, 1449 (2001)